Sixth International Symposium on Turbulence and Shear Flow Phenomena
Seoul, Korea, 22-24 June 2009

COHERENT STRUCTURES IN NEAR-WALL TURBULENCE

Sophie Herpin[1,2], Jean-Marc Foucaut[2], Julio Soria[1] and Michel Stanislas[2]

1: Laboratoire de Mécanique de Lille (LML)
Ecole Centrale de Lille
Bd Paul Langevin, Cite Scientifique, 59655 Villeneuve d'Ascq cedex, France

2: Laboratory for Turbulence Research in Aerospace and Combustion (LTRAC)
Monash University,
VIC 3800 Australia

ABSTRACT

Streamwise and spanwise vortices are investigated in a database of near-wall turbulence constituted of SPIV data of boundary layer covering a large range of Reynolds numbers ($Re_\theta \in [1300; 18950]$) and of a DNS dataset of channel flow at $Re_\tau = 950$. The detection algorithm is based on a fit of the velocity field surrounding extrema of swirling strength to an Oseen vortex. Some statistical results on the characteristics of the vortices (radius, vorticity, convection velocity, density) are investigated, giving some new insight into the organization of near-wall turbulence.

INTRODUCTION

Near-wall turbulence is organized into coherent structures which are believed to play a key role in the maintenance of turbulence. In particular, the streamwise and spanwise oriented vortices, through their ability to transport mass and momentum across the mean velocity gradient, are a fundamental feature of near-wall turbulence. The description, scaling laws and generation mechanism of these structures have been the focus of many studies, but still remain unclear. The present study aims at providing some new insight into these outstanding issues through the analysis of a SPIV database of turbulent boundary layer covering a large range of Reynolds numbers ($Re_\theta \in [1300; 18950]$) and of a DNS dataset of channel flow at $Re_\tau = 950$.

DESCRIPTION OF THE DATABASE

boundary layer flow

The boundary layer data was acquired by means of stereoscopic particle image velocimetry in two complementary flow facilities: the LTRAC water-tunnel in Melbourne (Australia) and the LML wind-tunnel in Lille (France). The characteristics of the database (size of the field of views, interrogation window, and mesh spacing) are summarized in table (1). A brief summary is given below.

The measurements in the LTRAC water-tunnel were realized in a streamwise/wall-normal (X-Y) plane of a turbulent boundary layer at moderate Reynolds numbers ($Re_\theta = 1300$ and 2200). The free-stream turbulence intensity in the water-tunnel is relatively high, on the order of $2.6\%U_e$ and $5.4\%U_e$ for the measurements at $Re_\theta = 1300$ and $Re_\theta = 2200$ respectively. Extensive details on the experimental procedure and qualification of the data can be found in Herpin et al (2008) and Herpin (2009). The data feature low measurement uncertainty (0.75% of the free stream velocity on the in-plane velocity components, and 1.5% on the out-of plane component), large spatial dynamic range (thanks to the large CCD array of the PCO 4000 camera), and high spatial resolution (with an interrogation window size of 15^+ and a mesh spacing of 4.5^+ on average).

The measurements in the LML wind-tunnel were realized both in a streamwise/wall-normal (X-Y) plane and in a spanwise/wall-normal (Y-Z) plane of a turbulent boundary layer at high Reynolds numbers (Re_θ=7800, 10140, 13420 and 18950). The description of the setup as well as the qualification of the data can be found in Herpin (2009). At all Reynolds numbers and in both planes, the measurement feature low uncertainty ($0.7\%U_\infty$ for all velocity components) and high spatial resolution (with an IW size varying from 11.2^+ to 20.6^+ and a mesh spacing from 3.2^+ to 6^+ depending on the Reynolds number).

channel flow

The data of turbulent channel flow is from DelAlamo et al (2006) and was obtained by means of direct numerical simulation (DNS). The characteristics of the full DNS are summarized in table 2(a). The detection was run on streamwise/wall-normal and spanwise/wall-normal planes of this DNS, interpolated on a regular mesh. The planes were extracted from nine three-dimensional velocity fields, uncorrelated in time. Successive planes are separated by a distance equal to h^+ for the XY planes and to $h^+/2$ for the YZ planes (where h is the half channel height). The interpolation was undertaken using two-dimensional bi-cubic spline interpolation. The regular mesh have a spacing of 4.5^+ in all directions. This resolution is close to the native resolution of the DNS in the spanwise direction, and is equal to the one of the LTRAC dataset. It can be seen that the native mesh spacing of the DNS in the streamwise direction is more than twice as large as the spacing used for the interpolation. In contrast, the full DNS was better resolved in the wall-normal direction. The characteristics of the interpolated XY and YZ planes of the DNS are summarized in table 2(b). The total number of points for the DNS planes (over the two spatial directions and over the number of samples) is approximately equal to the total number of points for the SPIV dataset at $Re_\theta = 2200$.

(a) Full DNS from DelAlamo et al (2006)

Re_τ	S_x	S_y	S_z	Δx^+	Δy^+	Δz^+
950	$8\Pi h$	$2h$	$3\Pi h$	11	variable	5.7

(b) interpolated planes

Plane (1-2)	h^+ Re_τ	Domain $S_{x/z}, S_y$	Mesh step Δ_i	n° records
XY	950	$8\Pi h$, h	4.5^+	342
ZY	950	$3\Pi h$, h	4.5^+	468

Table 2: Characteristics of the the DNS dataset

AVERAGE PROPERTIES OF THE DATABASE

The wall normal evolution of the mean streamwise velocity was computed by averaging the data over the number of sample acquired and over the homogeneous directions (x for the XY plane,

facility	Plane (1-2)	Re_θ	δ^+ Re_τ	Domain S_1, S_2	L_{IW}	Mesh step Δ_i	1st point	n° records
LTRAC	XY	1300	820	4δ, 1.4δ	15.2^+	4.7^+	$y^+ = 15$	605
LTRAC	XY	2200	1390	2.6δ, 0.75δ	14.2^+	4.3^+	$y^+ = 15$	1815
LML	XY / YZ	7630	2590	0.15δ, 0.6δ	16.8^+	3.9^+	$y^+ = 24$ / $y^+ = 34$	3840 / 2048
LML	XY / YZ	10140	3620	0.08δ, 0.28δ	11.2^+	3.2^+	$y^+ = 13$ / $y^+ = 17$	4096 / 4096
LML	XY / YZ	13420	5020	0.08δ, 0.28δ	15.4^+	4.5^+	$y^+ = 15$ / $y^+ = 27$	4096 / 4352
LML	XY / YZ	18950	6860	0.08δ, 0.28δ	20.6^+	6.0^+	$y^+ = 20$ / $y^+ = 33$	3840 / 4608

Table 1: Characteristics of the LML and LTRAC database

z for the YZ plane). For the boundary layer flow, only the profiles obtained in the XY plane are shown, the profiles in the YZ plane showing the same overall behavior (except the position of the first valid point in the wall-normal direction, see table 1). For the channel flow, the mean profile was computed by DelAlamo et al (2006) on the full DNS (see table 1(a)).
It is plotted in external units (non dimensionalized with the free velocity U_e and the momentum thickness θ) in figure 1(a) and in wall units with a logarithmic scale in the near-wall region (scaled with the friction velocity U_τ and the viscosity ν) in figure 1(b).
In the outer region ($y/\delta \geq 0.2$), the boundary layer data display a good collapse in external scaling (figure 1(a)), and a different behavior of the channel flow data is visible. In the inner region ($y/\delta \leq 0.2$), all the data (both boundary layer and channel flow) display a very good collapse in wall-units, and is in excellent agreement with the law of the wall defined by the Van Driest law (for $0 < y^+ < 55$) and the logarithmic law (for $55 < y^+$ and $y/\delta < 0.2$).

Spectral analysis is a tool of special interest for the analysis of turbulence which is, in essence, a multi-scale phenomenon. Here we consider only the one-dimensional power spectra of the streamwise velocity $E_{11}(k)$ along the streamwise and spanwise direction, at $y^+ = 100$. It is computed as the product of the Fourier transform of the u velocity (after a periodization of the field for the SPIV data) times its complex conjugate, divided by the length of the field, and averaged over the number of samples and the homogeneous direction. The streamwise spectra $E_{11}(k_x)$ are shown in figure 2, and the spanwise spectra in figure 3, in an inner scaling (scaled with the distance to the wall y and the friction velocity U_τ, see Perry et al (1986)). As it can be seen, the SPIV spectra and the DNS spectra are in excellent agreement in the low ($\bar{k} < 1$) and intermediate ($1 < \bar{k} < 10$) wavenumbers range. In particular, all spectra tend to a slope of '-5/3' in the inertial subrange. In the high wavenumber domain, a spurious lift-up of the PIV spectra with respect to the DNS spectra is visible: it indicates that the effect of measurement noise dominates the effect of spatial averaging over the interrogation window (Foucaut et al (2004)). Taking the DNS spectrum as the reference spectrum of the flow, it is possible to compute the wavenumber $\bar{k}_{SNR=1}$ at a signal-to-noise-ratio of 1 (and the associated structure size, e.g. radius of a vortex that would be resolved with SNR=1, $r^+_{SNR=1} = \frac{1}{2}\frac{2\Pi y^+}{\bar{k}_{SNR=1}}$) (Herpin et al (2008)). The cut-off wavenumbers are reported on the spectra. Their values read: $\bar{k}_{SNR=1} = 12.7$ ($r^+_{SNR=1} = 25$) for the LTRAC datasets, $\bar{k}_{SNR=1} = 15.2$ ($r^+_{SNR=1} = 21$) for the LML datasets in the XY plane, and $\bar{k}_{SNR=1} = 16.6$ ($r^+_{SNR=1} = 19$) for the LML dataset in the YZ plane.

DETECTION TECHNIQUE

The different methods for identifying vortex cores in velocity vectors fields obtained from PIV or DNS have been reviewed in great details by Jeong and Hussain (1995) and Chakraborty et al (2005).

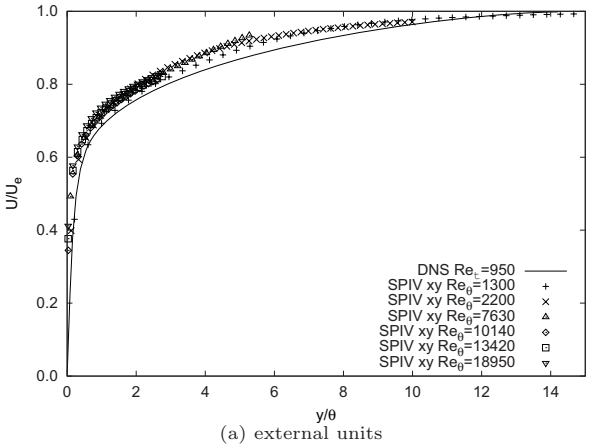

(a) external units

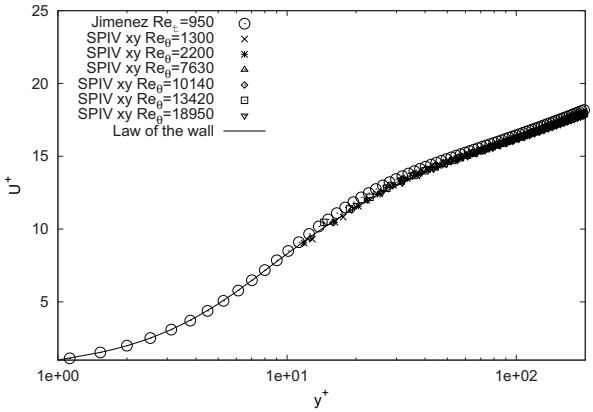

(b) wall units

Figure 1: Wall-normal evolution of mean longitudinal velocity

Local detection techniques based on the 3D velocity gradient tensor $A_{ij} = \frac{\partial u_i}{\partial x_j}$ (the Δ criterion Chong and Perry (1990)) present the advantage of being Galilean invariant. They have been successfully used to detect vortices in turbulent boundary layer. Because the database used in the present contribution is planar, the detection technique employed is based on the 2D velocity gradient tensor. This tensor is computed using a second order least-square derivative scheme that minimizes the propagation of measurement noise (Raffel et al (1998), Foucaut and Stanislas (2002)). When complex eigenvalues of the tensor exist, their imaginary part, called the swirling strength, is used as a detection function of vortex cores. This function is first normalized by the wall-normal profile of its standard deviation (as suggested by DelAlamo et al (2006) and Wu and Christensen (2006)), and then smoothed using a 3*3 sliding average to remove the remaining noise. Extrema exceeding a fixed threshold ($\lambda_{ci}(x_{1/3}, x_2) > 1.5\lambda_{ci,RMS}(x_2)$) are

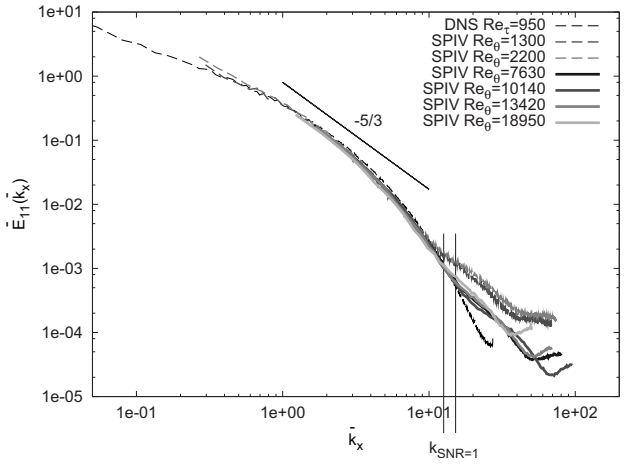

Figure 2: Longitudinal spectrum of u velocity at $y^+ = 100$

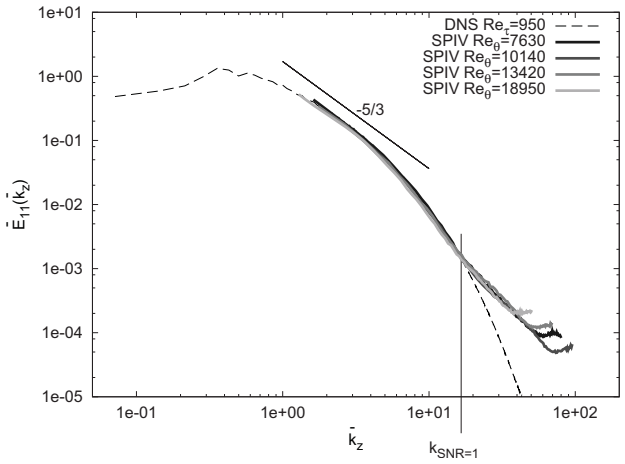

Figure 3: Spanwise spectrum of u velocity at $y^+ = 100$

retained as center of vortex cores.
The velocity fields surrounding extrema of the detection function are then fitted to a model vortex with a non-linear least square algorithm (Levenberg-Marquardt). The model is an Oseen vortex, defined in equation 1.

$$\vec{u}(r,\theta) = \vec{u_c} + \frac{\Gamma}{2\Pi}\frac{1}{r}\left(1 - exp\left(-\left(\frac{r}{r_0}\right)^2\right)\right)\vec{e_\theta} \qquad (1)$$

This procedure has already been employed by Carlier and Stanislas (2005) and Stanislas et al (2008). It validates that the structure detected is indeed a vortex, and allows the retrieval of the vortex characteristics (radius, circulation, convection velocity, sub-grid position of the center) through the fitted parameters of the model. An example of accepted vortex is shown in figure 4. It is plotted against the closest Oseen vortex obtained with the fitting procedure (the correlation coefficient between the model and the PIV field is 0.96).

RESULTS: CHARACTERISTICS OF THE VORTICES

The detection technique described above is employed to detect streamwise vortices (in the YZ planes) and spanwise vortices (in the XY planes) in the SPIV boundary layer database. It is also applied to the DNS planes interpolated on a regular mesh (see table 1(b)). Some statistics are computed on the characteristics of the detected vortices. The wall-normal evolution of the mean radius, vorticity, convection velocity and density are obtained by taking into account eddies contained in layers of 25^+ in height.

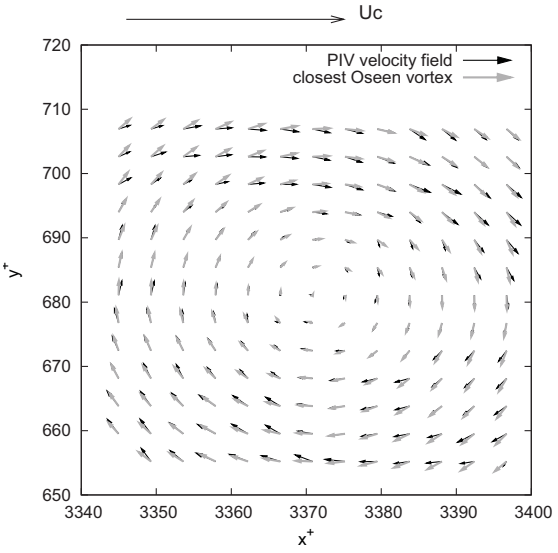

Figure 4: Comparison of a vortex and its closest Oseen model . The convection velocity (shown in black at the top of the figure) has been subtracted to the PIV velocity field.

Density of the vortices

The vortex densities are normalized such that they represents the densities per wall-unit square. At given orientation of the measurement plane, all datasets of the LML database show the same trend with wall-normal distance, and the only difference in the vortex densities is a shift in absolute value due to the effect of spatial resolution (some small vortices are not detected). Hence only the densities obtained in both planes in the boundary layer data at $Re_\theta = 10140$ (the highest spatial resolution) and in the channel flow at $Re_\tau = 950$ are shown (in figures 5 and 6 respectively). The total density of spanwise vortices (detected in the XY plane), the density of prograde (spanwise vortices with rotation in the same senses as the mean shear $w_0 < 0$) and retrograde ($w_0 > 0$) vortices, and the total density of streamwise vortices (detected in the YZ plane) are represented.

In the region $y^+ < 150$, the streamwise oriented vortices (detected in the YZ plane) are more numerous than the spanwise oriented vortices (detected in the XY plane). The fact that quasi-streamwise vortices are the major constituent of the near-wall region was also observed using a λ_2 criterion by Jeong et al (1997) in a DNS of channel flow at $Re_\tau = 180$ and by Sheng et al (2008) in holographic 3D velocity field of a turbulent boundary layer at $Re_\tau = 1400$. The wall-normal location where the density of the streamwise vortices reaches a maximum is obtained at $y^+ \approx 60$. After this maximum is reached, the density of streamwise vortices decreases rapidly with increasing wall-normal distance. This behavior of the streamwise vortices density in the near-wall region is in good agreement with the findings of Stanislas et al (2008) in SPIV measurements of a turbulent boundary layer at $Re_\theta = 7800$. The density of the spanwise vortices, in contrast, continuously increases from the wall up yo $y^+ \approx 150$ where a maximum is reached. Among the spanwise vortices, the predominance of the prograde vortices is overwhelming. Both prograde and retrograde forms increases with increasing wall-normal distance, but at very different rates: the increase is very fast for the prograde vortices, and rather slow for the retrograde ones. This suggest that different mechanism are responsible for their formation.

In the outer region ($y^+ > 150$), the vortex densities behave differently. First, it is of interest to note that the vortices population is now almost equally constituted of streamwise and spanwise vortices. The density of both vortices decreases at a medium rate with increasing wall-normal distance. Again, the prograde and the retrograde vortices follow different evolutions: the density of the prograde vortices continuously decreases with increasing

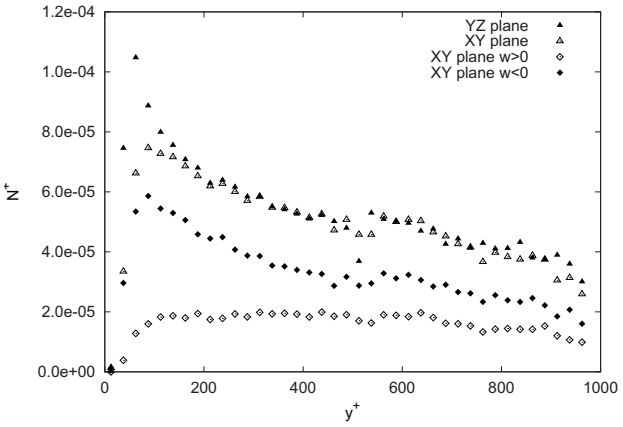

Figure 5: Density of vortices in the SPIV dataset at $Re_\theta = 10140$

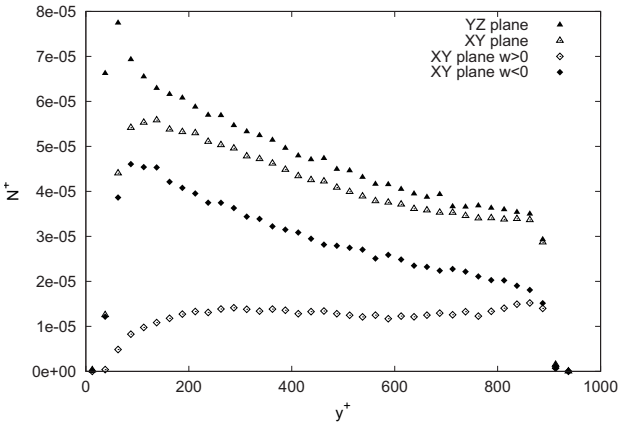

Figure 6: Density of vortices in the DNS dataset at $Re_\tau = 950$

wall-normal distance, while the density of the retrograde vortices stabilizes until $y/\delta = 0.5$, and then start to increase again, at a very low rate. It is worth noting that, in the DNS dataset, the density of prograde and retrograde vortices tends to an equal level at the channel centerline. This behavior of the prograde and retrograde vortices is in good agreement with the findings of Wu and Christensen (2006).

Radius of the vortices

The wall-normal evolution of the mean radius for all Reynolds numbers is plotted in figure 7 for the XY plane, and in figure 8 for the YZ plane, in wall units. It is of interest to note that, within each measurement plane, the wall-normal evolution of mean radius in wall units of the datasets at $Re_\tau = 950$, $Re_\theta = 2200$, 7630 and 13420 (which feature the same spatial resolution, see tables 1 and 2) are in excellent agreement. On a different note, the dataset at $Re_\theta = 10140$ (with the highest spatial resolution) display smaller values of mean radius, and the dataset at $Re_\theta = 18950$ (with the lowest spatial resolution) higher values of mean radius.

In the XY plane, the radius appears to be slowly increasing with wall normal distance over the whole field for all Reynolds numbers, except for the dataset at $Re_\theta = 1300$ where a steep increase of mean radius is observed for $y^+ > 400 \Leftrightarrow y/\delta > 0.5$. This may be due to intermittency with the free stream; in any case the spanwise vortex density in this region is quite low, cf previous paragraph. The behavior of the mean radius in the interpolated DNS dataset of turbulent channel flow appears to be similar to that of the PIV datasets in turbulent boundary layer, and in particular to that of the LTRAC dataset at $Re_\theta = 2200$. Close to the wall ($y^+ \approx 50$), the mean radius is about 20^+ on the dataset with the highest spatial resolution ($Re_\theta = 10140$) which is comparable

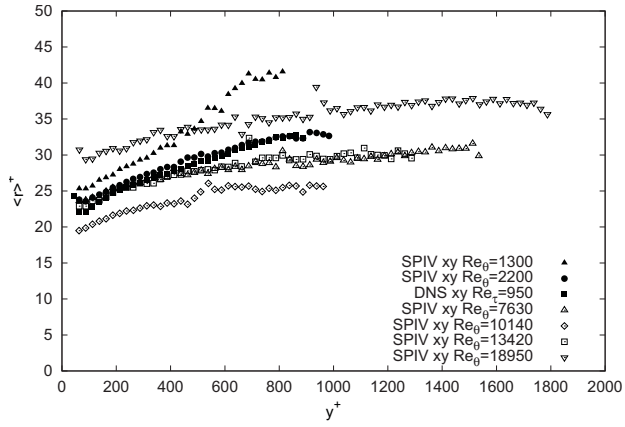

Figure 7: Mean radius of the spanwise vortices (XY plane), in wall-units

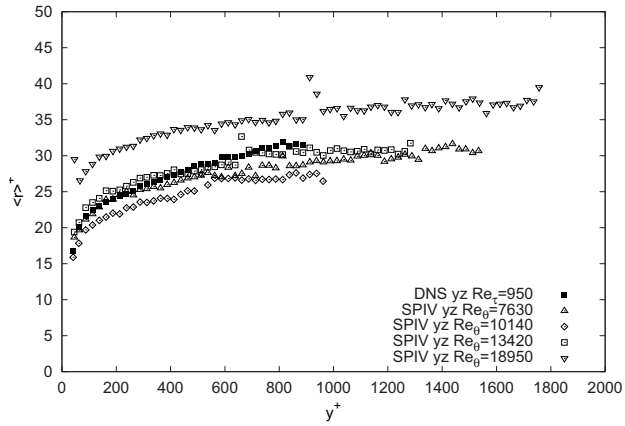

Figure 8: Mean radius of the streamwise vortices (YZ plane), in wall-units

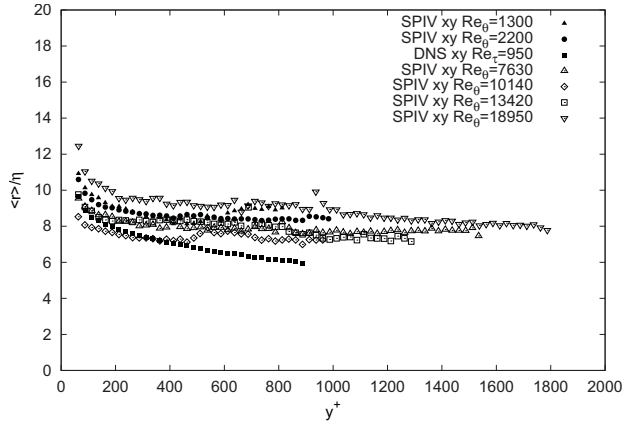

Figure 9: Mean radius in the XY plane, in Kolmogorov units

to the findings of Carlier and Stanislas (2005) at $Re_\theta = 7500$.
In the YZ plane, the behavior of the mean radius is quite different. Two regions must be distinguished: the region $y^+ < 100$, where the radius increases strongly with wall-normal distance, and the region $y^+ > 100$, where the radius increases slowly with wall-normal distance. This composite behavior in the YZ plane was also observed in Stanislas et al (2008) at $Re_\theta = 7800$ and $Re_\theta = 13420$. Close to the wall ($y^+ \approx 50$), the radius is as small as 15^+ on the dataset with the highest spatial resolution ($Re_\theta = 10140$), which is is excellent agreement with the estimation of Sheng et al (2008) for the radius of the streamwise vortices in the upper buffer layer. Therefore the streamwise vortices (detected in the YZ plane) are

found to be smaller than the spanwise vortices (detected in the XY plane) in the near wall region. This may indicate that, being inclined to the wall, the streamwise vortices are stretched by the mean velocity gradient. In the region $y^+ > 100$, the mean radius of the streamwise and spanwise vortices are comparable and slowly increase with increasing wall-normal distance toward a value of 25^+.

The wall-normal evolution of the mean radius scaled with the Kolmogorov length scale is plotted in figure 9 for the XY plane. The influence of the spatial resolution is less noticeable in this representation, and the mean radius at all Reynolds numbers is in quite good agreement. It is roughly independent of wall-normal distance for $y^+ > 150$ and equal to 8η, except for the channel flow data. In the YZ plane (not shown here), the behavior is the same except that the mean radius is found to be y independent over the full region of investigation (and not only for $y^+ > 150$).

Vorticity of the vortices

The wall normal evolution of the absolute mean value of vorticity at the center of the vortices is represented in figure 10 for the XY plane and in figure 11 for the YZ plane, in wall units. As it can be seen, in both planes, the vorticity decreases exponentially with the wall normal distance. In the near wall region ($y^+ < 250$) a good collapse of the vorticity in all datasets and in both planes is observed. The peak of vorticity at the wall is slightly higher in the YZ plane than in the XY plane. This may indicate that the streamwise vortices (detected in the YZ plane) are more intensified by the mean velocity gradient than the spanwise vortices (detected in the XY plane). Away from the wall ($y^+ > 250$), the mean vorticity of the vortices in the DNS dataset decreases more rapidly with wall-normal distance than in the SPIV dataset. Among the SPIV datasets, a good universality is observed for the streamwise vortices detected in the YZ plane, but some differences are visible for the spanwise vortices detected in the outer region of the XY plane, maybe owing to Reynolds number effects.

The wall-normal evolution of the mean vorticity scaled with the inverse of the Kolmogorov time scale is plotted in figure 12 for the XY plane. The behavior is similar in the two planes. The quantity $< w_0 > \tau$ appears to be quite constant in the upper buffer layer and in the logarithmic region of the SPIV datasets ($< w_0 > \tau \approx 1.4$), and both in the logarithmic region and outer region of the DNS dataset ($< w_0 > \tau \approx 1.6$).

Convection velocity

The convection velocity of the vortices detected in the XY plane and in the YZ plane is analyzed for all the datasets of the database. For each plane orientation, the in-plane components of the convection velocity are retrieved through a fit of a convected Oseen vortex to the local in-plane velocity field (see equation 1), while the out-of-plane component is retrieved as the velocity at the position of the fitted center of the vortex. It was checked that for all conditions, the vortices are convected with the mean streamwise velocity on average. The wall-normal evolution of the standard deviation of the three components of the vortices convection velocity in the LML database is shown in figure 13 for the vortices detected in the XY plane (spanwise vortices) and in figure 14 for the vortices detected in the YZ plane (streamwise vortices). The RMS of the velocity $u_i'^+$ at $Re_\theta = 7630$ is used for comparison.

Overall, it can be seen that the vortex data follow the velocity data for all Reynolds numbers and in both measurements planes. Wu and Christensen (2006) plotted the histogram of the streamwise convection velocity fluctuations of vortices detected in the XY plane of a channel flow at $Re_\tau = 1760$ and of a boundary layer at $Re_\tau = 2350$, and found that the width of these histograms was proportional to the local RMS streamwise velocity.

Besides this overall good agreement between $u_{c,i}'^+$ and $u_i'^+$, some

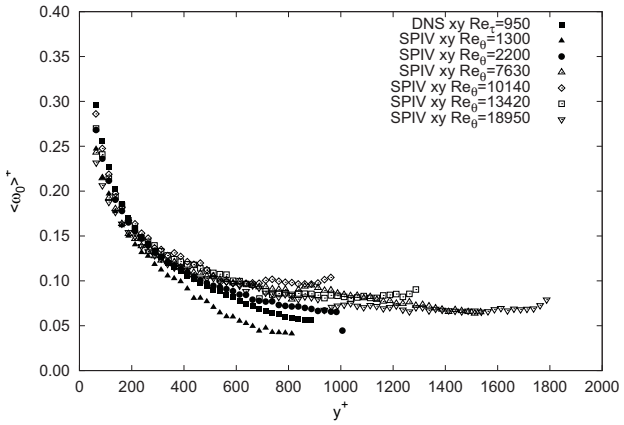

Figure 10: Mean vorticity of the spanwise vortices (XY plane), in wall-units

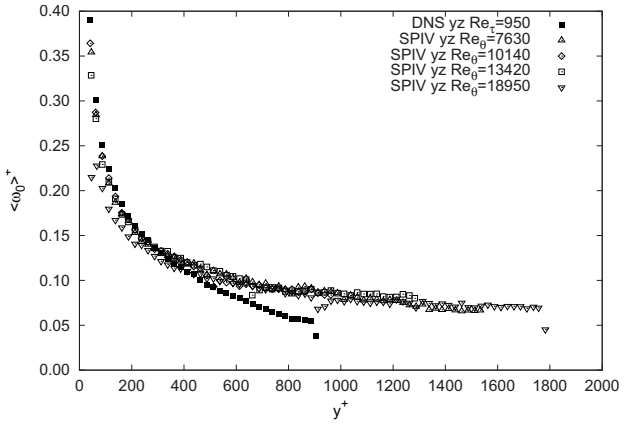

Figure 11: Mean vorticity of the streamwise vortices (YZ plane), in wall-units

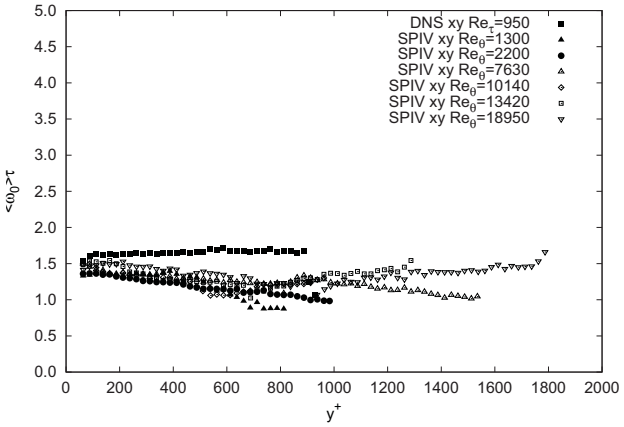

Figure 12: Wall-normal evolution of the mean vorticity in the XY plane, in Kolmogorov units

small differences appear in the present data:

- in both planes, the standard deviation of the in-plane convection velocity (the u and v component for the XY plane and the v and w components for the YZ plane) is found to be lower than the local turbulence level, especially in the near wall region ($y/\delta \in [0; 0.05]$). This may indicate that the vortices are more stable in place than the surrounding flow;
- in the XY plane, the standard deviation of the spanwise velocity at the center of the vortices is slightly higher than the local turbulence level, especially in the very near-wall region ($y/\delta \in [0; 0.05]$) where a peak is observed. This component is parallel to the axis of the vortices, and hence the

peak in RMS velocity may be indicative of some stretching/compression phenomenon;

- in the YZ plane, the standard deviation of the streamwise velocity is in good agreement with the local turbulence level, except that the near-wall peak is not retrieved;

These trends for the vortices detected in the XY plane are confirmed by the datasets in the lower Reynolds number range ($Re_\theta = 1300$, $Re_\tau = 950$ and $Re_\theta = 2200$), not shown here.

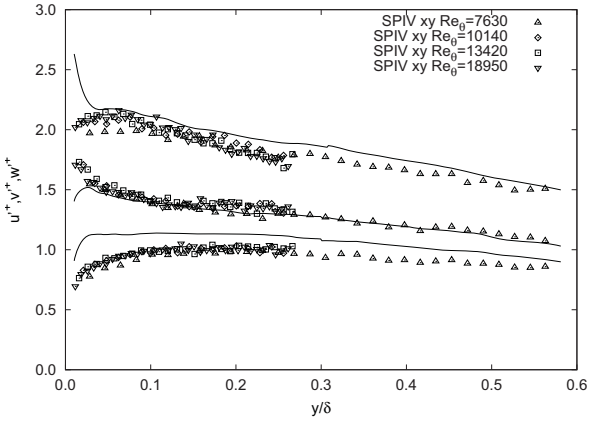

Figure 13: Standard deviation of the convection velocity of the spanwise vortices detected in XY plane (points), compared to that of the velocity in the dataset at $Re_\theta = 7360$ (solid line)

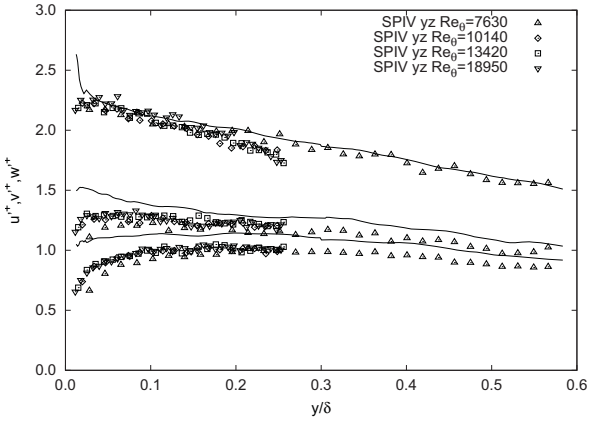

Figure 14: Standard deviation of the convection velocity of the streamwise vortices detected in YZ plane (points), compared to that of the velocity in the dataset at $Re_\theta = 7360$ (solid line)

CONCLUSION

A coherent structure detection was undertaken on the SPIV database of boundary layer flow at $Re_\theta \in [1300; 18950]$, as well as on a DNS dataset of channel flow at $Re_\tau = 950$. It is found that the structures are convected with the mean velocity and a standard deviation following that of the surrounding flow, but at a lower level indicating that the vortices are on average more stable than their environment. At all Reynolds numbers, the near-wall region is the most densely populated region, predominantly with streamwise vortices that are on average smaller and more intense than spanwise vortices. In contrast, the logarithmic region is equally constituted of streamwise and spanwise vortices having equivalent characteristics. In the outer region, some differences between the datasets are observed depending on the scaling employed: the wall-units scaling or the Kolmogorov scaling. In wall-unit scaling, a good universality in Reynolds numbers is observed in the near-wall and logarithmic region: the vorticity is found to be maximum at the wall, decreasing first rapidly and then slowly with increasing wall-normal distance; the radius is increasing slowly with wall-normal distance in both regions, except for the streamwise vortices for which a sharp increase in radius is observed in the near-wall region. The wall-units scaling is found to be deficient in the outer region, where Reynolds number effects are observed. In contrast, the Kolmogorov scaling appears to be universal both in Reynolds number and wall-normal distance across the three regions investigated, with a mean radius on the order of 8η and a mean vorticity on the order of $1.5\tau^{-1}$.

Acknowledgment

We are thankfull to “Campus International sur la Sécurité et l’Intermodalité dans les Transports (CISIT)” and to the Australian Research Council (ARC) for their financial support.
*

References

Carlier J, Stanislas M (2005) Experimental study of eddy structures in a turbulent boundary layer using particle image velocimetry. J Fluid Mech 535:143–188

Chakraborty P, Balachandar S, Adrian R (2005) On the relationships between local vortex identification schemes. J Fluid Mech 535:189–224

Chong MS, Perry AE (1990) A general classification of three-dimensional flow fields. Phys Fluids 5:765–777

DelAlamo JC, Jiménez J, Zandonade P, Moser RD (2006) Self-similar vortex clusters in the turbulent logarithmic region. J Fluid Mech 561:329–358

Foucaut JM, Stanislas M (2002) Some considerations on the accuracy and frequency response of some derivative filters applied to particle image velocimetry vector fields. Meas Sci Technol 13:1058–1071

Foucaut JM, Carlier J, Stanislas M (2004) PIV optimization for the study of turbulent flow using spectral analysis. Meas Sci Technol 15:1046–1058

Herpin S (2009) Study of the influence of the reynolds number on the organization of wall-bounded turbulence. PhD thesis, Ecole Centrale de Lille and Monash University

Herpin S, Wong CY, Stanislas M, Soria J (2008) Stereoscopic PIV measurements of a turbulent boundary layer with a large spatial dynamic range. Exp Fluids 45:745–763

Jeong J, Hussain F (1995) On the identification of a vortex. J Fluid Mech 285:69–94

Jeong J, Hussain F, Schoppa W, Kim J (1997) Coherent structures near the wall in a turbulent channel flow. J Fluid Mech 332:185–214

Perry AE, Henbest S, Chong MS (1986) A theoretical and experimental study of wall turbulence. J Fluid Mech 165:163–199

Raffel M, Willert C, Wereley ST, Kompenhans J (1998) Particle image velocimetry – a practical guide, 1st edition. Springer, Germany

Sheng J, Malkiel E, Katz J (2008) Using digital holographic microscopy for simultaneous measurements of 3d near wall velocity and wall shear stress in a turbulent boundary layer. Exp Fluids 45:1023–1035

Stanislas M, Perret L, Foucaut JM (2008) Vortical structures in the turbulent boundary layer: a possible route to a universal representation. J Fluid Mech 602:327–342

Wu Y, Christensen KT (2006) Population trends of spanwise vortices in wall turbulence. J Fluid Mech 568:55–76